metals

Article

Cold Compaction Behavior of Unsaturated Titanium Hydride Powders: Validation of Two Compaction Equations

Liu Luo, Yuchu Sun and Yongbai Tang *

College of Materials Science and Engineering, Sichuan University, Chengdu 610065, China
* Correspondence: tangyongbai@163.com

Abstract: Unsaturated titanium hydride (TiH_X) powder has high formability and is a promising raw material for titanium-based powder metallurgy. In this work, TiH_2, TiH_X, and HDH Ti powders were characterized, the cold compaction behavior of the powders was investigated, and the densification mechanism was analyzed. The TiH_X was a three-phase mixture containing an α plastic phase and δ and ε brittle phases through Rietveld refinement. The TiH_X compacts had compressive strength of over 420 MPa (higher than TiH_2 and similar to HDHTi) and relative density of over 80% (higher than TiH_2 and HDH Ti) at 600 MPa. The Gerdemann–Jablonski and Cooper–Eaton equation were used to simulate the powder compaction curves and describe powder compaction behavior. The plastic deformation of TiH_X powder is greater than $TiH_{2,}$ and the particle rearrangement is greater than HDH Ti during cold compaction. Such compaction behavior of TiH_X causes an excellent green-strength–relative-density combination.

Keywords: titanium powder metallurgy; titanium-based powders; cold compaction; Gerdemann–Jablonski equation; Cooper–Eaton equation

check for updates

Citation: Luo, L.; Sun, Y.; Tang, Y. Cold Compaction Behavior of Unsaturated Titanium Hydride Powders: Validation of Two Compaction Equations. *Metals* **2023**, *13*, 360. https://doi.org/10.3390/met13020360

Academic Editor: Joan-Josep Suñol

Received: 14 January 2023
Revised: 4 February 2023
Accepted: 7 February 2023
Published: 10 February 2023

1. Introduction

Titanium and titanium alloys, being prestigious among lightweight materials owing to their unmatched mechanical properties, are crucial structural components in the aerospace, automobiles, and navigation industries [1,2]. The major challenge of these materials resides in the expensiveness that prohibits overall commercialization, which could be resolved by the deployment of the powder metallurgy (PM) technique [1,2]. Based on compaction and sintering, the process achieves better cost-effectiveness in comparison with cast/wrought titanium alloys [2,3].

Throughout the PM process, cold compaction was developed into a reliable and efficient technique aiming at cost and energy optimization [2,3]. Ensuring fine compaction of powder is the initial step of the PM process; this directly imposes an influence on green strength and, eventually, the mechanical properties of a sample part after sintering.

The compaction behavior of metal, ceramic, and pharmaceutical powders has been studied continuously, and several different descriptions of stages of densification mechanisms have been proposed to explain the phenomena observed during powder compaction. Seelig and Wulff describe the mechanism in three stages, as particle packing, elastic and plastic deformation, and cold working and fragmentation [4]. Since Walker first related green density to compaction pressure to describe the compaction process [5], many compaction equations have been derived. The compression equations applied to titanium and titanium-base powder are as follows: Heckel [6], Kawakita and Ludde [7], Panelli-Filho [8], Ge [9], Shapiro [10], Gerdemann–Jablonski [4] and Cooper–Eaton [11]. Among them, the Gerdemann–Jablonski equation, as well as Cooper–Eaton equation, which showed a good fit to experimental data in the pressure range, have been proposed to describe the compaction mechanisms.

Researchers have shown continued interest in the cold compaction behavior of titanium and titanium-based powder due to the development of low-cost titanium PM.

Hydride–dehydride (HDH) Ti powder, similar to other ductile metal powders, exhibits the characteristic of plastic deformation during the pressing process [12–16]. In contrast, the density of titanium alloy prepared with HDH Ti powder has only reached about 95% [17]. In addition to the studies developed for HDH Ti powder, selecting TiH_2 powder as feedstock instead of HDH Ti powder, titanium alloys with low oxygen content and high density were obtainable [17–20]. Unlike pure titanium powder, the compaction behavior of TiH_2 powder appears closer to a ceramic material due to its low strength and brittleness; during compaction, particle rearrangement, fracture, and fragmentation are involved in the cold pressing process rather than plastic deformation [21–24]. Although TiH_2 PM has many advantages, TiH_2 applied as raw material still exhibits certain defects, containing TiH_2 showing unappealing strength, and showing vulnerability of green compact on edge drop and crack; these are especially significant during the preparation of parts having large-scale and high structural complexity [25]. A solution to these issues was discussed by Wei et al. by application of unsaturated titanium hydride (TiH_X, $0 < X < 2$) powder raw material in replacement of TiH_2 [25]. Green compact made from TiH_X powder had higher green strength compared to HDH Ti and TiH_2 powders.

In this study, the powder characteristics and compaction behavior of HDH Ti, TiH_2, and TiH_X powders were investigated. From the perspective of mathematical fitting and physical description, the validity of two nonlinear compaction equations used in the field of powder metallurgy for the compaction behavior of the above three powders was evaluated, and a more reliable explanation of the compaction mechanism was provided.

2. Materials and Methods

In this study, TiH_2, TiH_X, and HDH Ti powders were used. The TiH_2 powder was obtained by crushing hydrogenated titanium sponge and then sieving into 325–150 mesh. The hydrogenated sponge titanium was obtained by activating titanium sponge(Panzhihua Steel Enterprise Xinyu Chemical Co., Ltd., Panzhihua, China) under vacuum (within 10^{-2} Pa) at 420 °C for 1 h in a tube reactor (Sichuan University, Chengdu, China), then completely absorbing hydrogen in an ultrapure hydrogen (99.999%) atmosphere, and, finally, cooling to room temperature. The TiH_2 powder then underwent dehydrogenation in a vacuum furnace (Shanghai Chenhua Electric Furnace Co., Ltd., Shanghai, China) at a pressure of 10^{-3} Pa to produce TiH_X and HDH Ti powders. The process parameters of the heat treatments for TiH_2 and TiH_X powders are given in Table 1.

Table 1. Parameters of heat treatments of individual samples.

Sample No.	Dehydrogenation Temperature (°C)	Dehydrogenation Time
TiH_2	0	0 min
Dehy-1	640	1 min
Dehy-2	640	5 min
Dehy-3	640	15 min
HDH Ti	640	4 h

Note: Dehy-1, Dehy-2, and Dehy-3 are the designation of TiH_X.

The particle size distributions (PSD) of the powder fractions were measured using a JL-1155 laser particle-size instrument (Chengdu Jingxin Powder Test Equipment Co., Ltd., Chengdu, China). The morphology of all the powders and green compacts was investigated with scanning electron microscopy (SEM) using Aztec X-Max (Oxford Instruments, Oxford, UK). The oxygen content of the powders was measured by the LECO ONH analyzer (LECO, San Jose, CA, USA). The crystal structures of the powders were identified with X-ray diffraction (EMPYREAN, PANalytical B.V., Almelo, Holland) using Cu-Ka radiation in air at room temperature under scanning profiles of 20° to 90° in 2θ range, 0.013° step angle, and 10 s duration per step angle (10 s per channel acquisition time). The XRD patterns were compared with known phases and analyzed using the JCPC standard diffraction database.

Rietveld refinement was used to analyze all XRD patterns for quantitative analysis of phase composition and determination of crystal structure and lattice parameters [26].

The compressibility test was performed to study the cold compaction behavior of powders following a procedure similar to that described in Gerdemann's work [4]. A 1.2 g quantity of each powder was uniaxially pressed to 650 MPa in a 10.0 mm cylindrical steel die using an Instron 5569 hydraulic universal testing machine (Instron, Norwood, MA, USA) with a punching speed of 1 mm/min and pressure changes recorded every 0.1 s. Before filling the cavity with powder, mold walls and plunger were wiped with a small amount of a 1:1 suspension of zinc stearate and absolute ethanol. The powder compact was then de-molded, and its mass, height, and diameter were measured. Finally, the green density for each applied load was obtained. Origin 9.0 software was used to fit experimental data with compaction equations and analyze the parameters.

Green strength was determined by a compressive strength test using an Instron 5569 hydraulic universal testing machine at a loading speed of 0.3 mm/min. The sample preparation method for the compression test was as follows: a 3 g quantity of each powder was uniaxially compacted with a four-column hydraulic press (34 SM-810 H-T, Chengdu Lux Hydraulic Manufacturing Co., Ltd., Chengdu, China) at a pressure of 600 MPa to achieve a cold compact with a height–diameter ratio of 1:1.

3. Results and Discussion

3.1. Powder Characterization

SEM was applied to observe the morphology of TiH_2, TiH_X, and HDH Ti powders; the shape of particles was found to be angular. Vacuum dehydrogenation has a negligible effect on the morphology of TiH_2 powder under low magnification (Figure 1a,b,d,e,g,h,j,k,m,n). Figure 1c displays micrographs of the cleaved surfaces at a higher magnification, showing the different structural planes of the TiH_2 powder. From observation of TiH_X powder presented in Figure 1f,i,l and HDH Ti powder shown in Figure 1o, the steps on the surface of the samples were found to be smoothened, indicating the critical effect brought to the morphology by dehydrogenation treatment. Similarity in surface morphology found between TiH_X and HDH Ti powders further validated the significance of dehydrogenation in this aspect.

The PSDs of all the powders are shown in Figure 2 and Table 2. The D_{10}, D_{50}, and D_{90} of all the powders show a tendency to decline during the ongoing hydrogen desorption process of TiH_X. Nonetheless, PSDs of all the powders remained similar, which suggested the effect of dehydrogenation on particle size was insignificant and was not considered within the scope of this work.

Table 2 lists the oxygen content of each powder. It has been verified that the dehydrogenation process of TiH_2 is accompanied with deoxidation [27], and the relatively lower oxygen content of HDH Ti and Dehy-1 powders compared with TiH_2 was considered to be a reflection of goodness for the process. However, the oxygen content of Dehy-2 and Dehy-3 was higher than that of TiH_2; further discussion on these phenomena is given in the XRD analysis below.

Table 2. Particle size distribution and oxygen content of TiH_2, Dehy-1, Dehy-2, Dehy-3 and HDH Ti powders.

Sample. No	PSD (μm)	D_{10} (μm)	D_{50} (μm)	D_{90} (μm)	Oxygen (wt%)
TiH_2	0–115	58.29	76.85	98.94	0.17
Dehy-1	0–115	37.27	75.27	98.95	0.14
Dehy-2	0–115	37.15	75.05	98.19	0.20
Dehy-3	0–115	36.76	74.68	98.14	0.23
HDH Ti	0–115	37.19	72.73	96.78	0.16

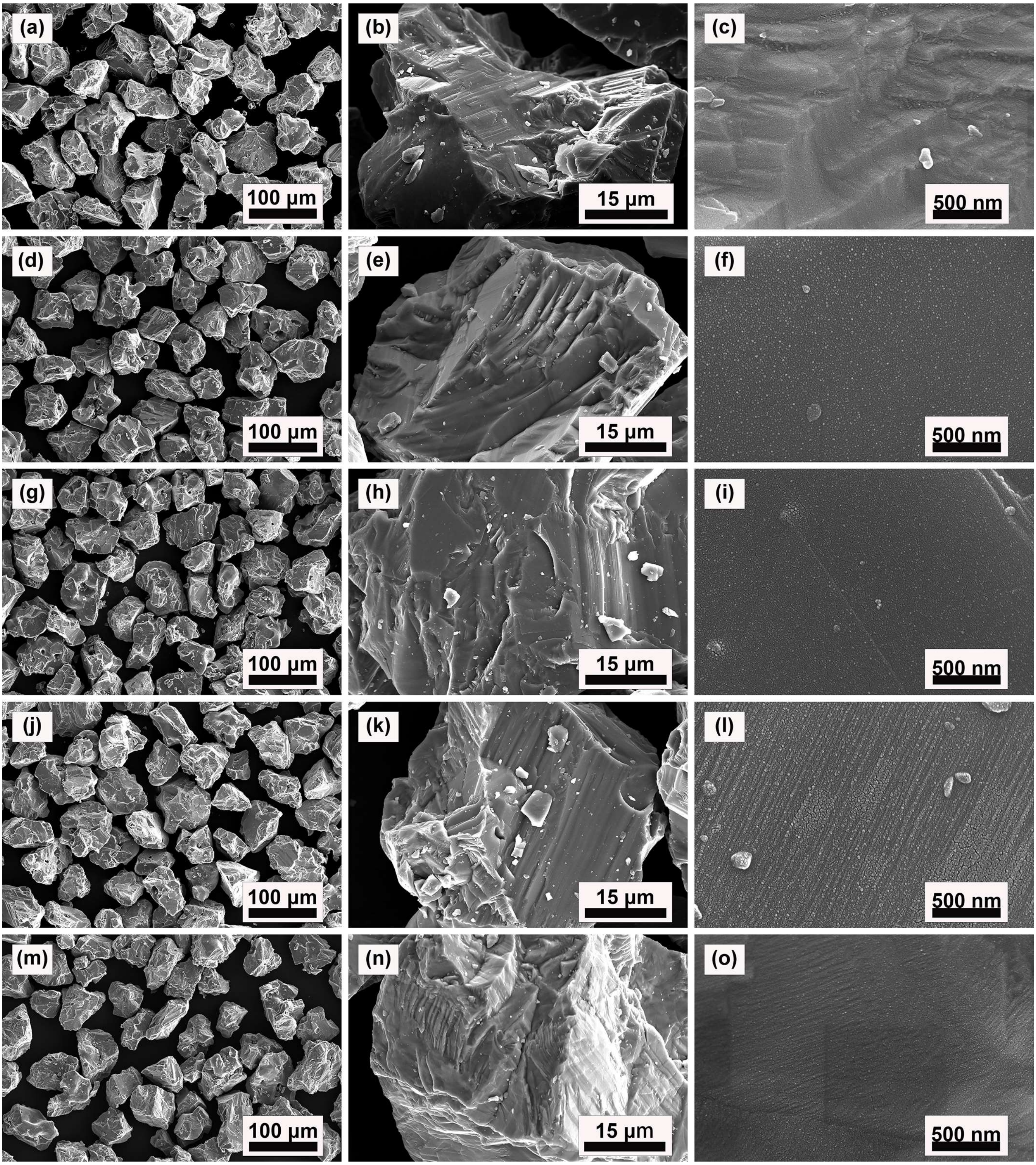

Figure 1. SEM images of the TiH_2 (**a**–**c**), the Dehy-1 (**d**–**f**), Dehy-2 (**g**–**i**), Dehy-3 (**j**–**l**), and HDH Ti (**m**–**o**) powders.

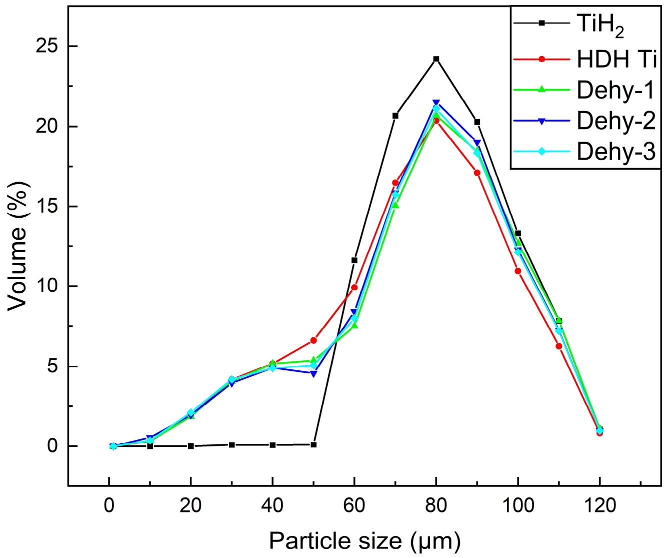

Figure 2. Particle-size distribution of the TiH_2, Dehy-1, Dehy-2, Dehy-3 and HDH Ti powders.

Figure 3 shows the XRD patterns of all the powders, and the corresponding crystallographic data are summarized in Table 3. From comparison with the XRD database, the TiH_2 powder was found to be a single phase. Using powder diffraction files, its composition was identified as δ phase of titanium hydride in face-centered cubic crystal structure with lattice parameter found to be a = 4.4500 Å. The HDH Ti powder after dehydrogenation also existed as a single phase, which was the α phase of Titanium (a = 2.9493 Å, c = 4.6822 Å) with hexagonal closest-packed crystal structure. All the TiH_X powders with different hydrogen concentrations showed the co-existence of the α phase, the δ phase, and the ε phase of titanium hydride. The ε phase has a face-centered tetragonal structure with c/a < 1. After dehydrogenation for 1 and 5 min, it was verified to be the dominant hydride phase, taking up 94% and 85% of the total hydride phase, respectively. In contrast, as dehydrogenation time prolonged to 15 min, the δ phase became the major phase, with the amount of phase reaching 54.92%. With the increase in dehydrogenation time, the phase content of the α phase increased gradually.

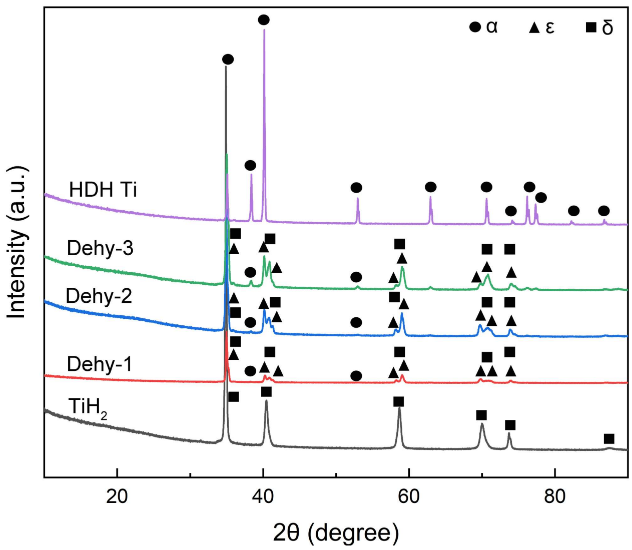

Figure 3. XRD patterns of the TiH_2, Dehy-1, Dehy-2, Dehy-3 and HDH Ti powders.

Table 3. Crystallographic data of the TiH_2, TiH_X, and HDH Ti powders based on Rietveld refinement analysis.

Sample. No	Theoretical Density (g/cm^3)	Phase Composition	Space Group	Portion (wt%)	Lattice Parameters (Å)		V (Å^3)
TiH_2	3.75	δ	F m-3 m	100.00	a	4.4500	88.1211
Dehy-1	3.79	δ	F m-3 m	3.00	a	4.4212	86.4189
		ε	I 4/m m m	95.61	a c	3.1663 4.3697	43.8074
		α	P 63/m m c	1.39	a c	2.9474 4.6533	40.4241
Dehy-2	3.85	δ	F m-3 m	9.55	a	4.4163	86.1335
		ε	I 4/m m m	84.30	a c	3.1638 4.3623	43.6661
		α	P 63/m m c	6.15	a c	2.9514 4.6708	40.6855
Dehy-3	3.89	δ	F m-3 m	54.92	a	4.4109	85.8199
		ε	I 4/m m m	31.31	a c	3.1614 4.3599	43.5763
		α	P 63/m m c	13.77	a c	2.9537 4.6757	40.7924
HDH Ti	4.51	α	P 63/m m c	100.00	a	2.9493	40.7270

The lattice constant and unit cell volume of the δ phase in all the TiH_X powders was smaller than that in TiH_2, since hydrogen atoms were released at elevated temperatures. For the case of the ε phase, known to be unstable in this process, its lattice and unit cell volume declined as the dehydrogenation process continued. Even though the unit volume of α decreased during desorption of hydrogen atoms, the influence of oxygen atoms on it is still dominant, because the volume of each hydrogen atom is much smaller than oxygen atoms. Considering the high affinity of oxygen to the α phase, the unit cell volume of the α phase could be increased by promoting α phase oxygen solid solution. Hence, the amount of oxygen solution was positively correlated with the α content, which explains why the oxygen content and the unit cell volume of α expanded as dehydrogenation kept proceeding. Theoretically, the HDH Ti powder after a complete dehydrogenation process would reduce the oxygen content of TiH_2 powder. However, experimental results suggested otherwise: higher oxygen content in Dehy-2, Dehy-3, and HDH Ti than Dehy-1 was detected; these deviations from theory might be caused by powder sample contamination. The above analysis shows that a certain amount of δ phase and ε phase is beneficial to resist oxygen pollution.

The theoretical density of TiH_2 is 3.75 g/cm^3, and the theoretical density of HDH Ti is 4.51 g/cm^3. For TiH_X, because it is composed of mixed phases, its theoretical density ($\rho_{theoretical}$) is calculated with Equation (1), according to the mass fraction and theoretical density of each phase:

$$\rho_{theoretical} = (w_\delta/\rho_\delta + w_\varepsilon/\rho_\varepsilon + w_\alpha/\rho_\alpha)/100 \quad (1)$$

The w_x and ρ_x (x replaced with α, δ, or ε) are the mass fraction and theoretical density of corresponding phases, which vary as the lattice of each phase changes with the removal of hydrogen atoms. The theoretical density of TiH_X, which was used in the calculation of relative density, increases with dehydrogenation time.

3.2. Green Compact Characterization

The morphologies of the upper surface of the green compacts of TiH_2, TiH_X, and HDH Ti powders after cold pressing under 600 MPa are shown in Figure 4. The bulk of green compacts were found to be filled with pieces of samples that were shattered during pressing, and there are no significant visual indicators of plastic deformation behavior in the TiH_2 compact. In fact, it was found that these prevailing cracks also developed into the inner sections of these particles. Generally, these phenomena suggest that the plastic deformation contribution is quite minor in the compaction process of TiH_2 powder, and the process is mainly dependent on the rearrangement of particles and their fragments.

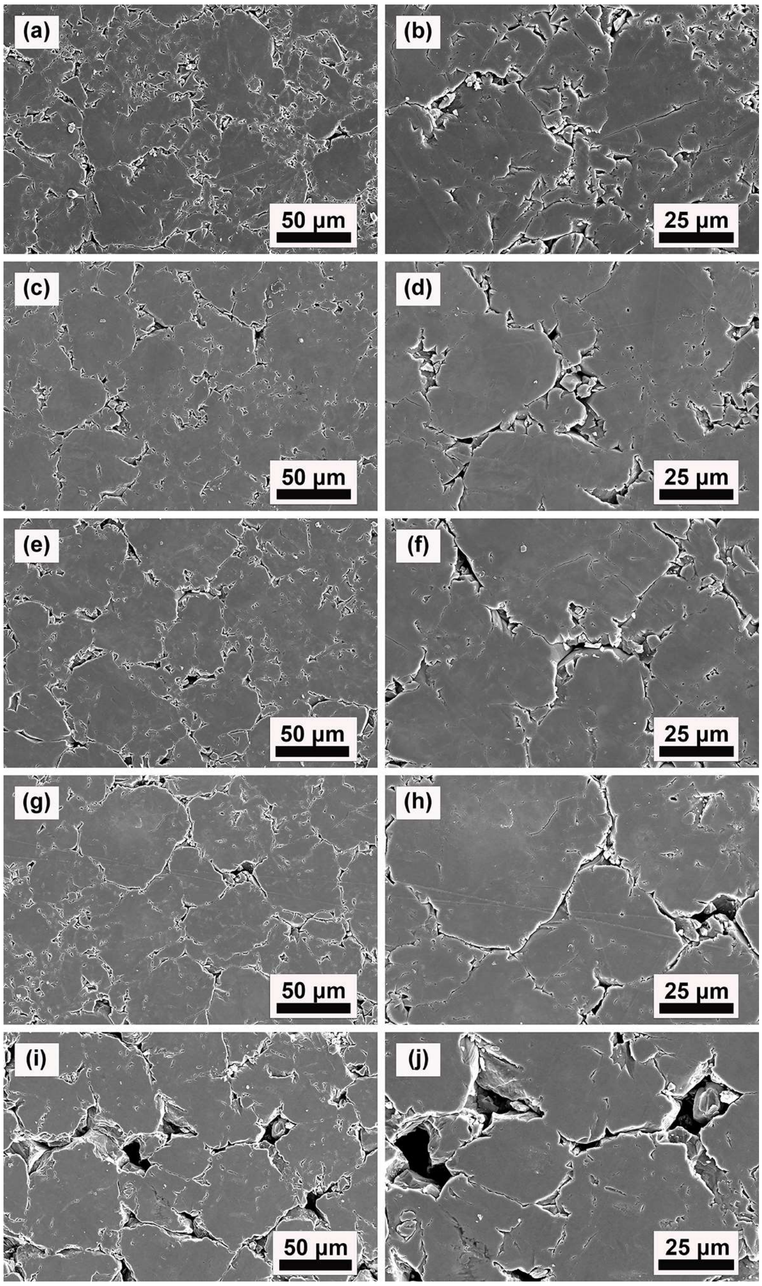

Figure 4. SEM images of the top surface of the TiH_2 (**a**,**b**), Dehy-1 (**c**,**d**), Dehy-2 (**e**,**f**), Dehy-3 (**g**,**h**) and HDH Ti (**i**,**j**) powders fraction-compacted at 600 MPa, showing regions of fracture, particle rearrangement and plastic deformation.

The morphologies of HDH Ti compact were found to contain fewer amounts of small-particle filling and inner-crack development than TiH_2 compact (Figure 4c,d). From its good mechanical meshing that determines particle bond strength, the fine plastic deformation of HDH Ti compact is confirmed. It conforms with the prediction that this material has a small probability of breaking at 600 MPa, and the compact would mainly develop by particle rearrangement as well as plastic deformation.

Figure 4e–j show the TiH_X compact morphologies; although crushing and cracking of particles produced considerable numbers of small particles, it is still milder compared to TiH_2 compact. Plastic deformation characteristics were found between particles, and finer plastic meshing between the particles was verified by the observations. The above analyses on morphologies suggest that the major densification mechanisms during TiH_x powder compaction are fragmentation and plastic rearrangement of particles.

The relative density vs compaction pressure for TiH_2, TiH_X, and HDH Ti powders is shown in Figure 5. Relative density of HDH Ti powder became the smallest, and relative densities of TiH_X powders were higher than the TiH_2 powder lots at 600 MPa. It can be seen from Figure 4d,e,h that TiH_X green compacts combine the advantages of filling in TiH_2 and meshing in HDH Ti. The excellent relative density obtained in the successive stage of pressing is achieved from fine-particle meshing and the mechanism of small particles filling into large ones. From the analysis of TiH_2, it was shown to maintain higher relative density than both TiH_X and HDH Ti before 100 MPa; after the pressure, its relative density became smaller than TiHX and HDH Ti. Hence, TiH_2 is brittle at low pressure and will produce small particles that promote rapid densification of itself.

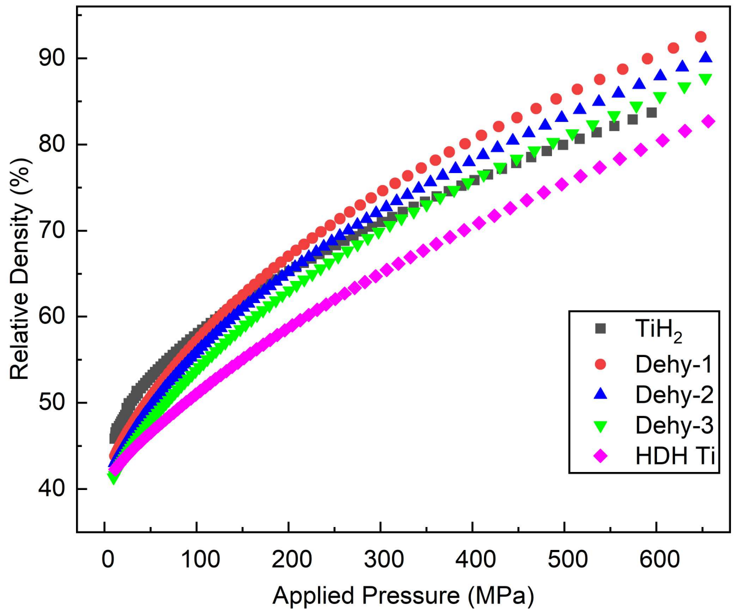

Figure 5. Relative density vs pressure of TiH_2, Dehy-1, Dehy-2, Dehy-3, and HDH Ti powders.

Apart from density, green strength determines the ability of green compact to retain its size and shape before the sintering process; this variable of the samples is identified by compressive strength, as shown in Figure 6. The compressive strength of TiH_X and HDH Ti green compacts was significantly better than that of TiH_2. It is commonly known that the brittleness of TiH_2 leads to poor powder formability. HDH Ti is a plastic material, which has higher formability than TiH_2, and the degree of particle plastic deformation is higher during powder compaction. The formability of the TiH_X compacts is more similar to or even higher than that of HDH Ti, which shows the advantage of the combination of the brittle phase (α) and the plastic phase (δ and ε). TiH_X powder, which has an outer layer of α phase, is really different from the fragile TiH_2 powder. The α phase provides TiH_X green compacts with higher particle strength and higher meshing strength between particles (plastic meshing between particles) than TiH_2. During the pressing process, the outer layer of TiH_X particles first resists the damage of external forces, and the outer layer maintains the high strength of the α phase until the outer layer breaks, so the TiH_X powder with only 1.39 wt % α phase also shows much higher compressive strength than TiH_2. The compressive strength of Dehy-2 was also slightly higher than HDH Ti, which is due to the possible buffering effect of δ and ε phases breaking during the pressing. However, the possibility of particle breakage decreases with the extension of dehydrogenation time, with the result that a further increase in α phase does not significantly improve compressive strength. Furthermore, the contribution of plastic deformation to improving compressive strength does not increase significantly with the increase in α phase, which will be seen in the compaction equations analysis.

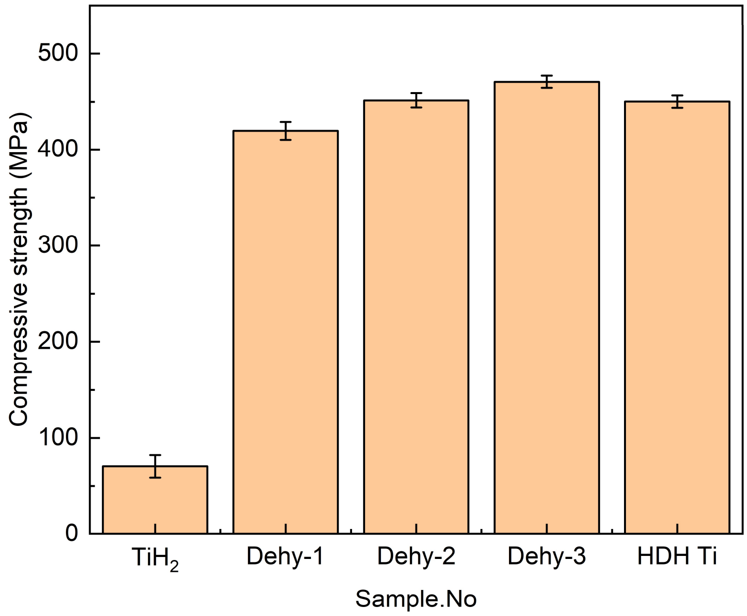

Figure 6. The Compressive strength of TiH_2, Dehy-1, Dehy-2, Dehy-3, and HDH Ti compacts.

3.3. Compressive Curve Fitting and Densification Mechanism Analysis

Numerous applications of various compaction equations showed that the Gerdemann–Jablonski equation and Cooper–Eaton equation achieve goodness of fit to the density–pressure relationship for titanium and titanium-based powders [15,16,28–30]. It is worth noting that parameters of the above two compression equations provide the significance of the contribution of different densification mechanisms.

3.3.1. Cooper–Eaton Equation

Cooper and Eaton described the pressing process as two processes in which powder fills pores. The first is to fill pores of the same size as the original particle, which mainly occurs due to the particles sliding against each other. This causes elastic deformation of particles and slight cracking, or plastic deformation sometimes occurs. The second process describes the filling of pores that are smaller than the original particles and could only be accomplished through plastic deformation or fragmentation. These two processes are represented by Equation (2),

$$V^* = \frac{V_0 - V}{V_0 - V_\infty} = a_1 \exp\left(-\frac{k_1}{P}\right) + a_2 exp\left(-\frac{k_2}{P}\right) \quad (2)$$

where V^* is the fractional volume of pores filling at applied pressure P, V_0 is the initial volume, V is the volume at applied pressure P, and V_∞ is the volume when all pores are filled. The dimensionless coefficients a_1 and a_2 represent the theoretical fraction of compaction that each particular process will achieve at infinite pressure. The coefficients k_1 and k_2 with units of pressure indicate the magnitude of the pressure where the associated process has the greatest probability.

Figure 7 shows the pore-volume reduction plotted vs the applied pressure, fitted to the Cooper–Eaton equation for all the powders under investigation. The results of fitting parameters are listed in Table 4. The Cooper–Eaton equation showed pretty good fit to experimental data, with an R-squared value exceeding 99.68%. According to the fitting data, the contribution of particle rearrangement on densification of TiH_2 powder is dominant, while plastic deformation in TiH_X and HDH Ti powders is considered the dominant mechanism of densification. At the same time, with the increase in powder dehydrogenation time, the contribution of plastic deformation to densification gradually increases. The densification at high pressure tends to be underestimated by Equation (2); the interpretation of compaction based on the parameters of the Cooper–Eaton equation seems quite similar to a realistic process, especially the cold compaction of the TiH_2 powder.

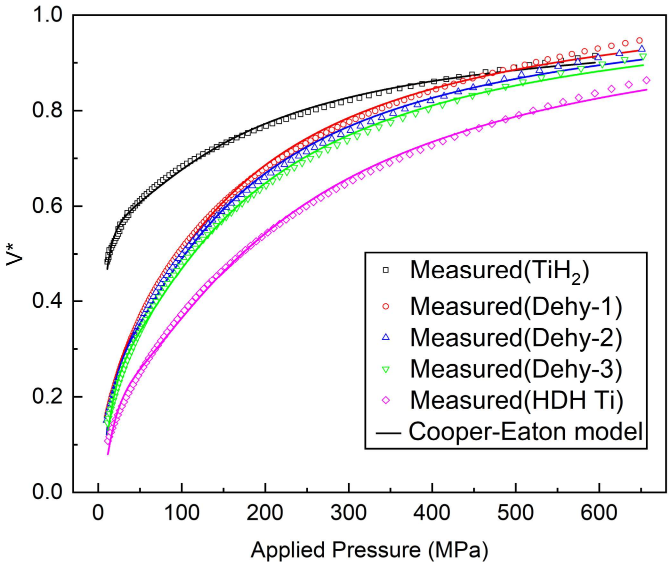

Figure 7. TiH_2, Dehy-1, Dehy-2, Dehy-3 and HDH Ti powders compaction data fitted according to Equation (2).

Table 4. Fit Parameters to Equation (2) for the Powder Materials Under Investigation.

Sample No.	Particle Rearrangement a_1	Particle Rearrangement k_1	Fragmentation/ Plastic Deformation a_2	Fragmentation/ Plastic Deformation k_2	Correlation Coefficient R^2	Particle Rearrangement/%	Fragmentation/Plastic Deformation/%
TiH_2	0.6419	3.4303	0.3583	185.7217	0.9968	64.18	35.82
Dehy-1	0.4434	13.0164	0.6412	172.7629	0.9986	40.88	59.12
Dehy-2	0.4315	12.8420	0.6327	174.8165	0.9982	40.55	59.45
Dehy-3	0.4272	14.2781	0.6349	186.2967	0.9986	40.22	59.78
HDH Ti	0.2971	11.4522	0.7442	204.9790	0.9968	28.53	71.47

Note: $Particle\ Rearrangement\ \% = \frac{a1}{a1+a2} \times 100\ \%$; $Fragmentation/\ Plastic\ Deformation\ \% = \frac{a2}{a1+a2} \times 100\ \%$

Figure 8 shows the plot of each term of Equation (2) within the whole range of applied pressure. Particle rearrangement also starts from the beginning of compaction, becoming strongly active up to an asymptote value and maintaining itself to densification. Another densification mechanism (fragmentation and/or plastic deformation) initiates at 50 MPa, increasing continuously up to completion.

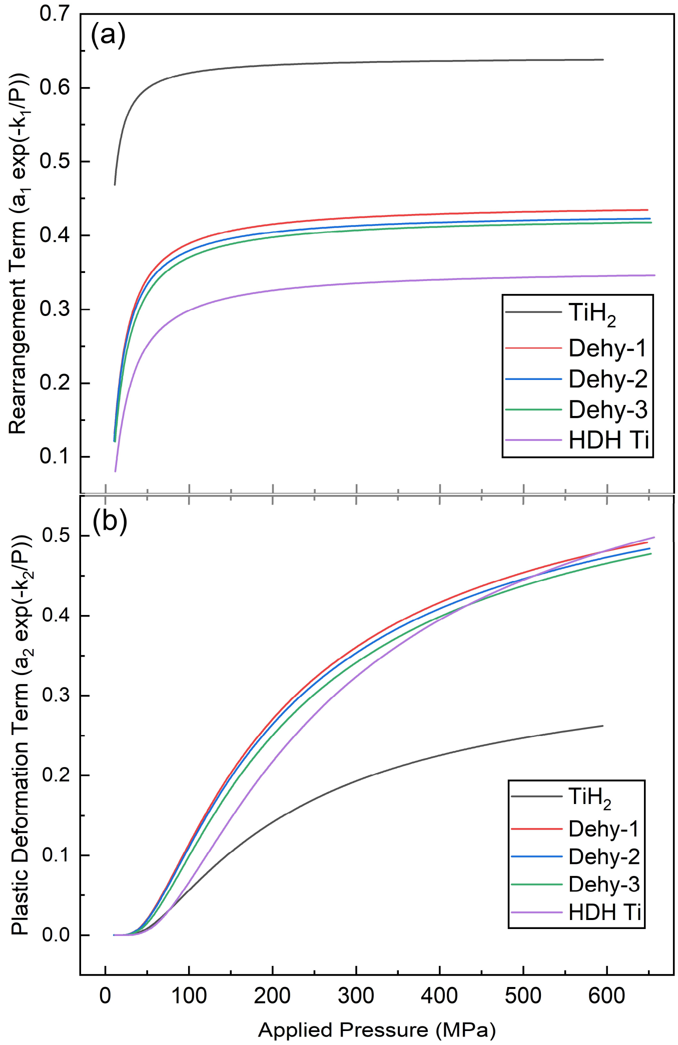

Figure 8. The contributions of particle rearrangement (**a**) and plastic deformation (**b**) mechanisms on densification according to Equation (2). The five powders are distinguished as follows: TiH_2, Dehy-1, Dehy-2, Dehy-3 and HDH Ti.

3.3.2. The Gerdemann–Jablonski Equation

Gerdemann and Jablonski incorporated three densification mechanisms of compaction into one simple equation. The equation is expressed as a constant (an initial density) and two independent first-order rate equations (particle rearrangement including sliding and fracture of the particles, and work hardening, including elastic and plastic deformation of particles). The three mechanisms are described in Equation (3),

$$D = D_0 + A(1 - exp(-aP)) + B(1 - exp(-bP)) \quad (3)$$

where D_0 represents an initial density, parameters A and B reflect the relative contribution of particle rearrangement and work hardening mechanisms, respectively, to densification; following Gerdemann and Jablonski, parameters a and b reflect the amount of pressure required to complete each mechanism. Ronald Machaka [16] evaluated the equation and pointed out that the equation is composed of two dynamic compaction mechanisms, namely, particle rearrangement and work hardening, and the initial density represents the initial condition rather than a mechanism for the entire compaction process.

Figure 9 is a plot of the true density vs applied pressure for all powders along with the fit to Equation (3). The fit parameters in Equation (3) for all the powders are tabulated in Table 5. An excellent fit ($R^2 > 99.95\%$) of Equation (3) was achieved to the data over the entire pressure range of the experiment. Table 5 shows the relative contribution of each densification mechanism to the overall final density. The HDH Ti powder has the relatively lowest contribution from the rearrangement term, and the TiH_X powder has a more significant contribution from the rearrangement mechanism. The contribution of the particle rearrangement term of TiH_2 powder to the overall densification is higher than that of TiH_X and HDH Ti powders.

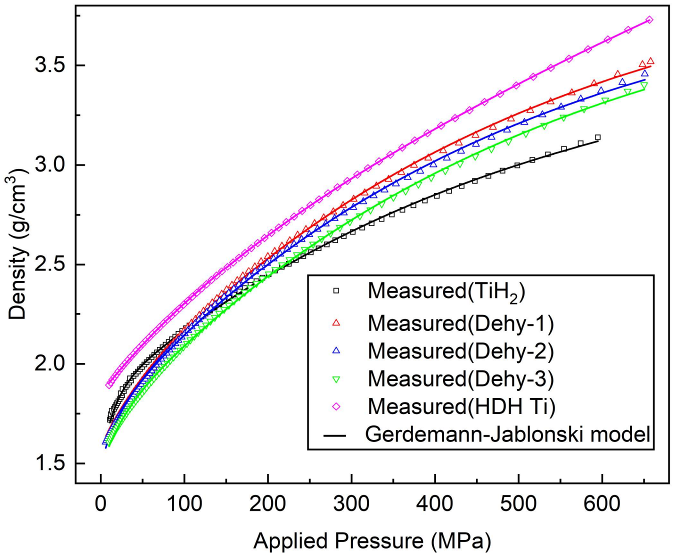

Figure 9. TiH_2, Dehy-1, Dehy-2, Dehy-3 and HDH Ti powders compaction data fitted according to Equation (3).

Table 5. Fit Parameters to Equation (3) for the Powder Materials Under Investigation.

Sample. No	Initial Density D_0	Particle Rearrangement A	a	Work Hardening B	b	Correlation Coefficient R^2	Particle Rearrangement/%	Work Hardening/%
TiH_2	1.510	0.3253	0.0605	1.8581	0.0020	0.9995	14.90	85.10
Dehy-1	1.498	0.2224	0.0431	2.3805	0.2224	0.9996	8.55	91.45
Dehy-2	1.496	0.2125	0.0480	2.3070	0.0021	0.9995	8.44	91.56
Dehy-3	1.471	0.1990	0.0426	2.3770	0.0020	0.9997	7.72	92.28
HDH Ti	1.770	0.1388	0.0658	2.9945	0.0014	0.9998	4.43	95.57

Note: *Particle Rearrangement* $\% = \frac{A}{A+B} \times 100\ \%$; *Work Hardening* $\% = \frac{B}{A+B} \times 100\ \%$

The two exponential terms of Equation (3), and how they vary with pressure, are also plotted individually within Figure 10. The particle rearrangement term rises rapidly and reaches an asymptote value at low applied pressure, and the asymptote value and its corresponding applied pressure value for each powder decline with the increase in powder dehydrogenation time. With the increase in pressure, the work hardening term gradually increases but does not reach an asymptotic value, and gradually dominates in the later stage.

In the Gerdemann–Jablonski equation, all the powders have a more significant contribution from the plastic deformation mechanism, which is very consistent with the compaction behavior of HDH Ti. Obviously, the compaction behavior of TiH_2 powder does not meet this point, and the Cooper–Eaton equation is more convincing; Sergio Luis Graciano Petroni [30] came to a similar conclusion. These two nonlinear equations accurately describe the changes in the compaction mechanism of different titanium-based powders. It is clearly shown in Tables 4 and 5 that the more the content of α plastic phase, the greater the contribution of plastic deformation to densification, and the more the content of brittle phases (δ and ε), the more obvious the particle rearrangement.

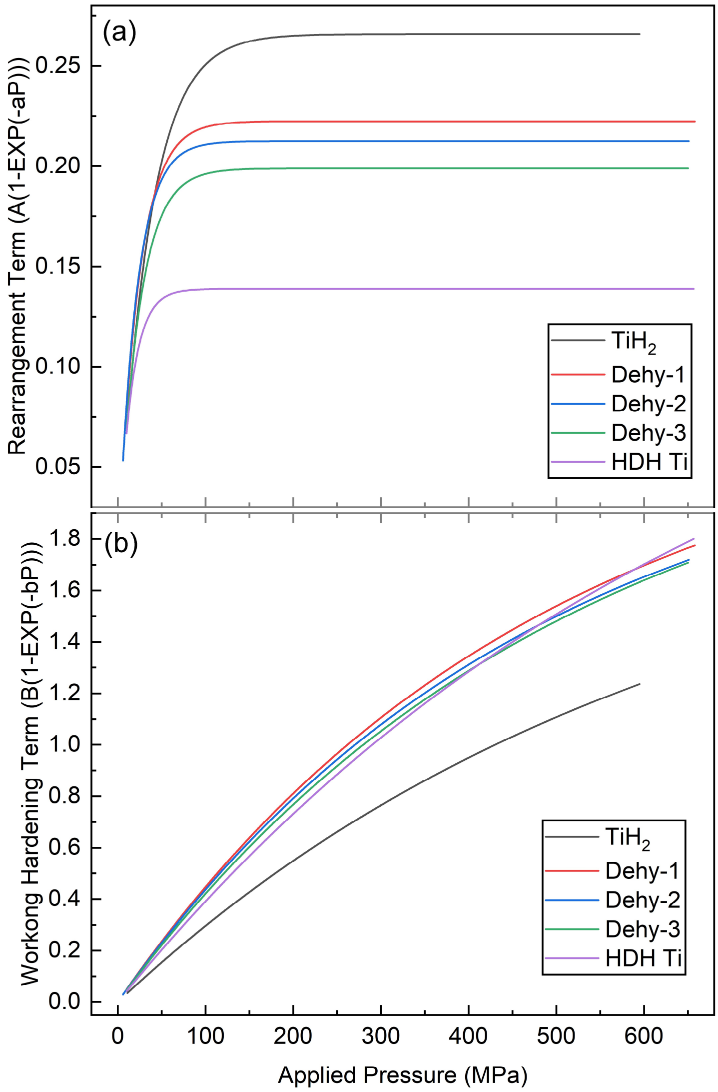

Figure 10. The contributions of particle rearrangement (**a**) and plastic deformation (**b**) mechanisms on densification according to Equation (3). The five powders are distinguished as follows: TiH_2, Dehy-1, Dehy-2, Dehy-3 and HDH Ti.

3.3.3. Analysis of the Densification Mechanism of Powder

TiH_2 is a typical brittle ceramic-like material, with particles undergoing only small and inadequate plastic deformation, followed by cracking at higher pressures. HDH Ti is typical of a ductile material, in which densification is mainly governed by plastic deformation. The contributions of particle rearrangement to densification are greater for all powders at lower pressures. Fragmentation and plastic deformation show greater contribution at intermediate and high pressures.

The presence of the α phase in TiH_X powder plays an important role in cold compaction, which provides the powder with more ability to go on to plastic deformation. The existence of titanium hydride phases (ε and δ phase) can make the powder more prone to fragmentation. Corresponding to the above equations, its particle rearrangement effect is still higher than that of HDH Ti. The relative density of the TiH_X green compact is higher than that of HDH Ti and TiH_2, which is due to its ability to cause particle breakage under low pressure and its plastic deformation ability to promote the densification process when particle breakage cannot contribute to densification under high pressure.

4. Conclusions

The powder characteristics and cold compaction behavior of TiH_X compared with TiH_2 and HDH Ti were investigated. The findings could be abridged as follows:

TiH_X was a three-phase mixture including α, δ, and ε phases. The effect of dehydrogenation on smoothing the cleavage surface of TiH_2 powder was seen in TiH_X and HDH Ti. The morphologies of TiH_X compacts were characterized by the gap between small particles filling large particles and the plastic meshing between particles. The TiH_X compacts could obtain compressive strength of more than 420 MPa (higher than TiH_2 and similar to HDHTI) and relative density of more than 80% (higher than TiH_2 and HDH Ti) at 600 MPa.

Gerdemann–Jablonski and Cooper–Eaton equations were found to be suitable to fitting powder compressibility curves. The above two equations accurately describe the change in cold compaction behavior caused by the change in phase composition of TiH_X; that is, the more α phase content, the greater the contribution of plastic deformation to densification, while the change in rearrangement is the opposite.

The TiH_X compacts possess both the filling advantage of TiH_2—that is, the brittle phases (δ and ε) produce particle breakage and make small particles fill the gap between large particles—and the meshing advantage of HDH Ti—that is, the existence of α plastic phase made strong bonding strength between particles. This is why an excellent green-strength—relative-density combination is obtained in TiH_X compact.

Author Contributions: L.L.: Writing—original draft, investigation, methodology, formal analysis; Y.S.: writing—review and editing; Y.T.: project administration, writing—review and editing, supervision. All authors have read and agreed to the published version of the manuscript.

Funding: This research was funded by Technological breakthroughs in technological achievements of titanium powder metallurgy products (No. 2018CDPZH-2).

Institutional Review Board Statement: Not applicable.

Informed Consent Statement: Not applicable.

Data Availability Statement: Data are available from the corresponding author on reasonable request.

Conflicts of Interest: The authors declare no conflict of interest.

References

1. Fang, Z.G.Z.; Paramore, J.D.; Sun, P.; Chandran, K.S.R.; Zhang, Y.; Xia, Y.; Cao, F.; Koopman, M.; Free, M. Powder metallurgy of titanium—Past, present, and future. *Int. Mater. Rev.* **2018**, *63*, 407–459. [CrossRef]
2. Qian, M.; Froes, F.H. *Titanium Powder Metallurgy: Science, Technology and Applications*; Butterworth-Heinemann: Waltham, MA, USA, 2015; pp. 1–628.
3. Kumar, P.; Chandran, K.S.R. Strength–Ductility Property Maps of Powder Metallurgy (PM) Ti-6Al-4V Alloy: A Critical Review of Processing-Structure-Property Relationships. *Met. Mater. Trans. A* **2017**, *48*, 2301–2319. [CrossRef]
4. Gerdemann, S.J.; Jablonski, P.D. Compaction of Titanium Powders. *Met. Mater. Trans. A* **2010**, *42*, 1325–1333. [CrossRef]
5. Walker, E.E. The properties of powders. Part VI. The compressibility of powders. *Trans. Faraday Soc.* **1923**, *19*, 73–82. [CrossRef]
6. Sonnergaard, J. A critical evaluation of the Heckel equation. *Int. J. Pharm.* **1999**, *193*, 63–71. [CrossRef]
7. Kawakita, K.; Lüdde, K.-H. Some considerations on powder compression equations. *Powder Technol.* **1971**, *4*, 61–68. [CrossRef]
8. Panelli, R.; Ambrozio, F. A study of a new phenomenological compacting equation. *Powder Technol.* **2001**, *114*, 255–261. [CrossRef]
9. Ge, R. A new powder compaction equation. *Int. J. Powder Met.* **1991**, *27*, 211–216.
10. Shapiro, I. Compaction of powders X. Development of a general compaction equation. *Adv. Powder Metall. Part. Mater.* **1993**, *3*, 229–243.
11. Cooper, A.R.; Eaton, L.E. Compation behavior of several ceramic powders. *J. Am. Ceram. Soc.* **1962**, *45*, 97–101. [CrossRef]
12. Dong, S.; Wang, B.; Song, Y.; Ma, G.; Xu, H.; Savvakin, D.; Ivasishin, O. Comparative Study on Cold Compaction Behavior of TiH_2 Powder and HDH-Ti Powder. *Adv. Mater. Sci. Eng.* **2021**, *2021*, 9999541. [CrossRef]
13. Esteban, P.G.; Thomas, Y.; Baril, E.; Ruiz-Navas, E.M.; Gordo, E. Study of compaction and ejection of hydrided-dehydrided titanium powder. *Met. Mater. Int.* **2011**, *17*, 45–55. [CrossRef]
14. Hadadzadeh, A.; Whitney, M.A.; Wells, M.A.; Corbin, S.F. Analysis of compressibility behavior and development of a plastic yield model for uniaxial die compaction of sponge titanium powder. *J. Mater. Process. Technol.* **2017**, *243*, 92–99. [CrossRef]

15. Lou, J.; Gabbitas, B.; Zhang, D.; Yang, F. Effects of Initial Powder Compact Thickness, Lubrication, and Particle Morphology on the Cold Compaction Behavior of Ti Powder. *Met. Mater. Trans. A* **2015**, *46*, 3646–3655. [CrossRef]
16. Machaka, R.; Chikwanda, H.K. An Experimental Evaluation of the Gerdemann–Jablonski Compaction Equation. *Met. Mater. Trans. A* **2015**, *46*, 2194–2200. [CrossRef]
17. Robertson, I.M.; Schaffer, G.B. Comparison of sintering of titanium and titanium hydride powders. *Powder Met.* **2010**, *53*, 12–19. [CrossRef]
18. Ivasishin, O.M.; Bondareva, K.; Bondarchuk, V.; Gerasimchuk, O.; Savvakin, D.; Gryaznov, B. Fatigue resistance of powder metallurgy Ti–6Al–4V alloy. *Strength Mater.* **2004**, *36*, 225–230. [CrossRef]
19. Ivasishin, O.M.; Savvakin, D.G. The Impact of Diffusion on Synthesis of High-Strength Titanium Alloys from Elemental Powder Blends. *Key Eng. Mater.* **2010**, *436*, 113–121. [CrossRef]
20. Robertson, I.M.; Schaffer, G.B. Review of densification of titanium based powder systems in press and sinter processing. *Powder Met.* **2010**, *53*, 146–162. [CrossRef]
21. Machio, C.; Machaka, R.; Chikwanda, H. Consolidation of titanium hydride powders during the production of titanium PM parts: The effect of die wall lubricants. *Mater. Des.* **2016**, *90*, 757–766. [CrossRef]
22. Machio, C.; Machaka, R.; Shabalala, T.; Chikwanda, H.K. Analysis of the Cold Compaction Behaviour of TiH2-316L Nanocomposite Powder Blend Using Compaction Models. *Mater. Sci. Forum* **2015**, *828–829*, 121–128. [CrossRef]
23. Ueta, M.C.C.; Fracote, C.A.; Henriques, V.A.R.; de Alencastro Graça, M.L.; Cairo, C.A.A. Densification Study of Titanium Powder Compacts. *Mater. Sci. Forum* **2005**, *498–499*, 211–216. [CrossRef]
24. Dong, S.; Ma, G.; Lei, P.; Cheng, T.; Savvakin, D.; Ivasishin, O. Comparative study on the densification process of different titanium powders. *Adv. Powder Technol.* **2021**, *32*, 2300–2310. [CrossRef]
25. Wei, Y.; Wang, C.; Zhang, Y.; Mei, L.; Xiao, S.; Chen, Y. The Compactibility of Unsaturated Titanium Hydride Powders. *J. Mater. Eng. Perform.* **2018**, *27*, 5752–5761. [CrossRef]
26. Rietveld, H.M. A profile refinement method for nuclear and magnetic structures. *J. Appl. Crystallogr.* **1969**, *2*, 65–71. [CrossRef]
27. Wang, C.; Pan, L.; Zhang, Y.; Xiao, S.; Chen, Y. Deoxidization mechanism of hydrogen in TiH2 dehydrogenation process. *Int. J. Hydrogen Energy* **2016**, *41*, 14836–14841. [CrossRef]
28. Dong, S.; Qiu, F.; Lei, P.; Cheng, T.; Ma, G.; Qu, L.; Ivasishin, O. Evaluation and parameter analysis of compaction equations applied to titanium powder. *Powder Met.* **2021**, *65*, 181–199. [CrossRef]
29. Machaka, R.; Chikwanda, H.K. Analysis of the Cold Compaction Behavior of Titanium Powders: A Comprehensive Inter-model Comparison Study of Compaction Equations. *Met. Mater. Trans. A* **2015**, *46*, 4286–4297. [CrossRef]
30. Petroni, S.L.G. PM compaction equations applied for the modelling of titanium hydride powders compressibility data. *Powder Met.* **2020**, *63*, 35–42. [CrossRef]